# UNIVERSAL, FLOW DEPENDENT RELATIVE PERMEABILITY SCALING FOR STEADY-STATE TWO-PHASE FLOWS IN POROUS MEDIA

Marios S. Valavanides
Dept. of Civil Engineering, University of West Attica, Campus 1, Ag. Spyridonos, Athens, GR-12210, Greece,

*This paper was prepared for presentation at the International Symposium of the Society of Core Analysts held in Trondheim, Norway, 27-30 August 2018*

## ABSTRACT

*The phenomenology of steady-state two-phase flow in porous media is recorded in the well-known relative permeability curves. Conventionally, relative permeabilities are considered as functions of saturation. Yet, this has been put into challenge by theoretical, numerical and laboratory studies of flow in artificial pore network models and real porous media that have revealed a significant dependency on the flow rates -especially when the flow regime is capillary to capillary/viscous and part of the disconnected non-wetting phase remains mobile. These studies suggest that relative permeability models should include the functional dependence on flow intensities.*

*Here, we present the outcome of extensive simulations implementing the DeProF true-to-mechanism model algorithm, in flow set-ups spanning 5 orders of magnitude, both in the capillary number, Ca, and the flow rate ratio, r, and for different favorable/unfavorable viscosity ratio systems in a typical pore network. The systematic dependence of the pressure gradient (and of the relative permeabilities) on the local flow rate intensities is revealed. This systematic dependence can be described analytically by a universal scaling functional form along the entire domain of the true independent variables of the process, Ca and r.*

*The proposed scaling opens new possibilities in improving SCAL measurements and implementing true-to-mechanism (flow-dependent) relative permeability maps in simulators.*

## INTRODUCTION

The conventional use of saturation as the independent variable in two-phase flow in porous media (PM) is based on the oversimplifying assumption that disconnected fluidic elements of the non-wetting phase (NWP) (ganglia and droplets) do not move with the average flow but remain stranded in the pore medium matrix. This situation arises when flow conditions of 'relatively small values' of the capillary number are maintained; in those cases the disconnected NWP fluidic elements block part of the available flow cross-section by a fraction analogous to the average saturation and effect a relative reduction of the permeability. Nevertheless, there is ample experimental evidence that disconnected flow is a substantial and sometimes prevailing flow pattern [1-10].

Treating relative permeabilities as functions of the saturation is inefficient in providing

a correct and specific-enough description of the process across the domain of all possible flow conditions. The issue is extensively discussed in [11].

A particular value in saturation does not necessarily imply that a unique disconnected structure (arrangement) of the NWP will settle-in. Disconnected structures of the NWP can be coarsely described by a spectrum of population density distributions, extending from distributions of 'many-and-small' fluidic elements (droplets and small ganglia) to 'fewer-and-larger' fluidic elements (small and large ganglia). For any one of those cases, the corresponding superficial velocity of the disconnected NWP would not necessarily attain the same value. The latter would be the result of the 'negotiation' over the mass and momentum balances between the two factors inhibiting the transport of each phase, viscosity and capillarity, within the particular PM structure and for the particular, externally imposed, flow conditions. As a consequence, the effective permeability of the wetting phase (WP) and the NWP for any two different cluster configurations (any two different population density distributions) of disconnected phase would differ and, therefore, the corresponding values of the relative permeability to the NWP would be different. Yet, those different values of the relative permeability would correspond to the same saturation value. A universal, saturation-dependent description would be weak.

In addition, during routine core analysis, saturation is measured indirectly and cannot be externally imposed directly; it is only through control of a combination of pressure difference and/or flow rate of the NWP or WP that the system will attain an average saturation. If one wants to consistently and systematically describe the process in the entire flow regime (extending across extreme values in the capillary number and the viscosity ratio), one has to consider those variables that describe the externally imposed conditions and contain macroscopic kinematic information, e.g. the superficial velocity of each phase or, equivalently, the capillary number and the flow rate ratio. Moreover, saturation cannot adequately (or uniquely) describe the flow conditions. This is because saturation alone brings no definite input to the momentum balance, therefore it is questionable if it can provide any information on the *kinetics* of the macroscopic flow.

Observations of single phase flows within pore networks confirm that the macroscale pressure gradient scales linearly with the superficial fluid velocity (Darcy's law). This seems to be a quite trustworthy modeling consideration in the case of two-phase flow as well, especially when very high superficial velocities are considered and capillary forces are negligible. However, at moderate/low velocities, when capillary forces are comparable to viscous forces, the macroscopic pressure gradient does not scale linearly with the flow rate. Experimental studies on steady-state two-phase flows in 2D glass-etched pore network models [1, 2, 3], in glass beads [4, 7, 8], in virtual 3D pore networks [12], in glass bead columns [13], as well as in sand-pack columns [14], revealed that the non-linear relation between pressure gradient and flow rate can be described by generic power laws with different exponent values. The discrepancy between the values of the scaling exponents is attributed to differences associated with (a) dimensionality of the pertinent variables (b) measurements pertaining to different flow conditions, (c) dimensionality of the NWP/WP/PM system properties. Therefore, it is worth the effort to examine if these 'different' observations can be integrated in a universal power law relating appropriate dimensionless variables of the process.

The novelty of the present work pertains to: (a) revealing the systematic dependency of the pressure gradient, and of the relative permeabilities, on the flow conditions, in the form of extensive maps spanning across orders of magnitude over the capillary number and the flow rate ratio; (b) constructing a universal scaling function (or law) that describes analytically the dependence of the pressure gradient, and relative permeabilities, on the flow conditions. That came as a result of extensive simulations spanning 5 orders of magnitude in both the capillary number and flow rate ratio, implementing the DeProF model algorithm. The latter is build around a true-to-mechanism, stochastic scale-up model for steady-state two-phase flows in pore networks [15]. The model itself is based on the concept of decomposing the entire flow into a mixture of 3 prototype flows (connected-NWP pathway flow, small and large ganglion dynamics, drop traffic flow) each with a different degree of disconnection of the NWP (see next sections) Significant and systematic changes in the mixing of the 3 prototype flows were exposed [15].

## BASICS OF STEADY-STATE 2-PHASE FLOW IN POROUS MEDIA

Consider the simultaneous, one-dimensional concurrent flow of a non-wetting phase and a wetting phase across a porous medium control surface, $\widetilde{A}$, at flow rates equal to $\widetilde{q}_n$ and $\widetilde{q}_w$ respectively. Corresponding pressure differences, are induced upon the two phases. The phenomenological fractional flow Darcy relations that describe the steady-state, fully developed process, whereby the pressure gradient is *common* in both fluids, is

$$\widetilde{U}_i = \frac{\widetilde{q}_i}{\widetilde{A}} = \frac{\widetilde{k}}{\widetilde{\mu}_i} k_{ri} \frac{\Delta\widetilde{p}}{\Delta\widetilde{z}} \quad i = n, w \tag{1}$$

Note that, in the conventional Darcy formulation pertaining to the description of fractional flows, apart from the flow rates and relative permeabilities, the pressure gradients, $\left(\Delta\widetilde{p}/\Delta\widetilde{z}\right)_i \quad i = n, w$, are also indexed to account for different values along the NWP and WP. Nevertheless, in steady-state conditions, especially when the flow is fully developed, both phases share a common macroscopic pressure gradient, $\left(\Delta\widetilde{p}/\Delta\widetilde{z}\right)$, and the indexing may be dropped-out (see Appendix I, eqn (I-2), in [11]).

In general, two-phase flow in pore networks is impeded by the combination of viscous and capillary forces. A relative measure of the viscous over the capillary forces is provided by the value of the capillary number, *Ca*, conventionally defined as

$$Ca = \widetilde{\mu}_w \widetilde{U}_w / \widetilde{\gamma}_{\mathrm{nw}} \tag{2}$$

where $\widetilde{\gamma}_{nw}$, the interfacial tension between the two phases.

The set of superficial velocities may be appropriately reduced and replaced by a set of dimensionless variables, i.e. the capillary number, *Ca*, and the N/W flow rate ratio,

$$r = \widetilde{q}_n / \widetilde{q}_w = \widetilde{U}_n / \widetilde{U}_w \tag{3}$$

where $\widetilde{\mu}_w$ is the viscosity of the WP and $\widetilde{\gamma}_{nw}$ is the NWP/WP interfacial tension.

In particular, when steady-state conditions develop, the flow rate ratio is equal to the mobility ratio (see Appendix I in [11])

$$r = \frac{U_n}{U_w} = \frac{1}{\kappa}\frac{k_{rn}}{k_{rw}} \tag{4}$$

where

$$\kappa = \tilde{\mu}_n / \tilde{\mu}_w \tag{5}$$

is the NWP/WP bulk viscosity ratio.

## PREDICTION OF STEADY STATE RELATIVE PERMEABILITIES

The mechanistic model *DeProF* for immiscible, steady-state two-phase flow in pore networks predicts the reduced macroscopic pressure gradient, given the capillary number, NWP/WP flow rate ratio and the properties of the NWP/WP/PM system [15]. The model is based on the concept of decomposition in prototype flows, hence the acronym *DeProF*. It takes into account the pore-scale mechanisms and the sources of non-linearity caused by the motion of interfaces, as well as other complex, network-wide cooperative effects, to estimate the conductivity of each class of pore unit cells in a statistical sense. It implements effective medium theory with appropriate expressions for pore-to-macro scale consistency for NWP and WP mass transport, to derive an implicit algebraic relation invoking the macroscopic pressure gradient, the capillary number, *Ca*, the flow rate ratio, *r*, the viscosity ratio, $\kappa$, the advancing and receding contact angles, $\theta_A^0$, $\theta_R^0$ (wettability), and a set of parameters that describe the geometrical, topological and structural characteristics of the pore network, $\mathbf{x}_{pm}$.

Using the *DeProF* model, one can obtain the solution to the problem of steady-state two-phase flow in porous media in the form of the following transfer function

$$x = x\left(Ca, r; \kappa, \theta_A^0, \theta_R^0, \mathbf{x_{pm}}\right) \tag{6}$$

where

$$x = -\left(\frac{\Delta\tilde{p}}{\Delta\tilde{z}}\right)\frac{\tilde{k}}{\tilde{\gamma}_{nw}Ca} = \frac{1}{k_{rw}} \tag{7}$$

is the reduced macroscopic pressure gradient, i.e. the actual pressure gradient divided by the pressure gradient of an equivalent one-phase flow of water at superficial velocity equal to $\tilde{U}_w$ [the 2nd component of the product in eqn (7).]. By definition, the reduced pressure gradient is essentially the inverse of the relative permeability of the WP. Using the equivalence between the flow rate ratio and the mobility ratio, eqn (4), we may recover the relative permeability of the NWP as

$$k_{rn} = \kappa r k_{rw} \tag{8}$$

In a recent work, extensive simulations implementing the *DeProF* algorithm have been carried out to derive maps that describe the dependence of the flow structure on the independent flow variables, namely the capillary number, *Ca*, and the flow rate ratio, *r*, or, equivalently, to the reduced, superficial velocities of NWP and WP [15]. The simulations span 5 orders of magnitude in *Ca* $(-9 \le \log Ca \le -4)$ and *r* $(-2 \le \log r \le 2)$ over sufficiently fine steps. Fluid systems with various –favorable and

unfavorable- viscosity ratios (9 in total), have been examined.

Predictions of the reduced pressure gradient, *x*, are presented in Figure 1 for a typical NWP/WP/PM system with viscosity ratio $\kappa = 1.5$. The diagrams furnish the projections of the $x_{ij}(Ca_i, r_j)$ predicted values on a constant log *Ca* (a) and log*r* (b) planes. Markers are connected into iso-*Ca* and iso-*r* groups.

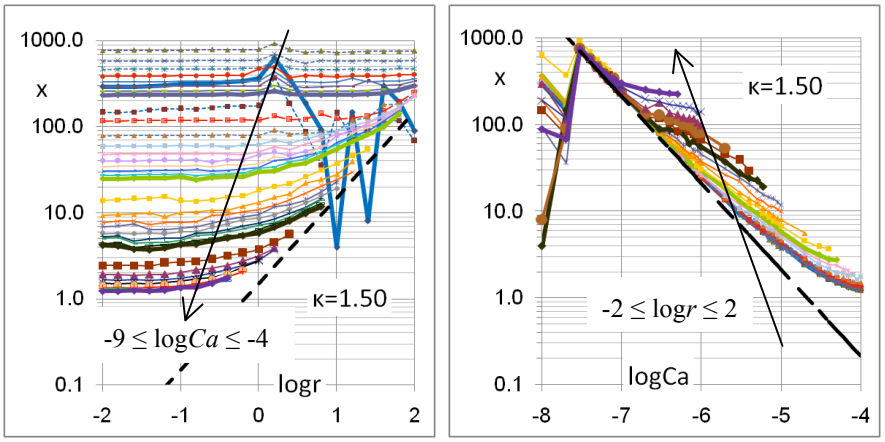


**Figure 1** Reduced pressure gradient values, *x*, for different values, (a) of the capillary number, *Ca*, and (b) of the flow rate ratio, *r*. Both diagrams pertain to a typical value of the viscosity ratio, $\kappa = 1.5$.

Referring to Figure 1(a) we observe that at the high-end of the flow-rate ratio domain, all curves pertaining to constant-*Ca* values tend to bundle and align asymptotically to a straight line (dashed), having the functional form

$$\log x = \log \kappa + \log r \quad \Leftrightarrow \quad x = \kappa r \tag{9}$$

Equation (9) states that at sufficiently large *Ca* values the reduced pressure gradient becomes a linear function of the flow rate ratio, with the linearity constant equal to the viscosity ratio. This is physically sound as, at high *Ca* values, capillarity effects fade away and the flow is regulated mainly by viscosity disparity, accounted by the viscosity ratio, $\kappa$. Essentially, what eq (9) describes is the decoupling between the flows of the NWP and the WP at very large flow rate values, $r \to \infty$. At this limit, we can recover a linear relation between the reduced pressure gradient and the flow rate ratio, eqn (9). The higher the *r* values, the earlier (in terms of *Ca* values) the approach to that decoupled-flow behavior /phenomenology, and the recovery of eqn (9).

We may observe a similar trend in Figure 1(b). At the low-end of the *Ca* domain, all iso-*r* curves tend to cluster /bundle and align asymptotically to a straight line with negative inclination. This asymptote is illustrated by the dashed line. Now the functional form is given by the expression, up to a constant, $Ca_0$,

$$\text{For } \log Ca << 0, \quad \log x = \log \kappa - \log Ca - \log Ca_0 \quad \Leftrightarrow \quad x = \frac{\kappa}{Ca_0 Ca} \tag{10}$$

This line extends down to a threshold value in *Ca*. For the NWP/WP/PM considered the threshold value is estimated at $\log Ca \approx -7.5$. Eqn (10) states that relative

permeability to the NWP drops down to a minimum, i.e. most of the NWP is immobile. Once more, eq (10) describes the decoupling between the flows of the NWP and WP at very low *Ca* values. The lower the value of flow rate ratio, *r*, the earlier (i.e. from higher *Ca* values) this asymptotic behavior is observed.

We will continue with deriving a universal function that can describe the dependence of the reduced pressure gradient -and of the relative permeabilities, on the independent variables of the process, the capillary number and the flow rate ratio.

## UNIVERSAL FUNCTIONAL FORM OF REL. PERMEABILITIES

The DeProF model predicted values $x_{ij}\left(Ca_i, r_j\right)$ of the reduced pressure gradient for different flow set-ups, i.e. different values of the capillary number, *Ca*, and the flow rate ratio, *r*, may be described by the universal scaling form

$$x\left(\log Ca, \log r\right) = A\left(\log Ca\right) + \kappa 10^{\log r} \tag{11}$$

where the functional $A\left(\log Ca\right)$ needs to be determined. We may implement least squares approximation fitting, to determine the values $A_i = A\left(\log Ca_i\right)$ pertaining to constant capillary number values, $\log Ca_i$,

$$A_i = \frac{1}{N_i}\left(\kappa \sum_{j=1}^{N_i} 10^{\log r_j} - \sum_{j=1}^{Ni} x_{ij}\right) \tag{12}$$

where $N_i$ is the number of detected points ($x_{ij}$) pertaining to the constant capillary number value, $Ca = Ca_i$. The set of ($A_i$, $Ca_i$) values is plotted on the diagram of Figure 2.

We may observe that the markers are lined-up against two straight line asymptotes; one with negative inclination and the other coinciding with the horizontal axis; these meet at an oblate angle. We may fit the set of $\left(\log Ca_i, \log A_i\right)$ values by a function of the form

$$\log Ca = x_0 + C_0 / \left(\log A\right)^2 + C_3 \log A \tag{13}$$

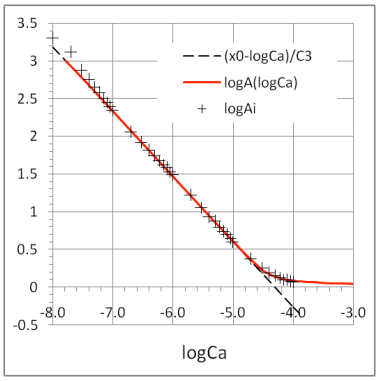


**Figure 2** Coefficient *A*, eqn (11). Markers fitted by function log*A*(log*Ca*), eqn (13)

where coefficient $C_0$ is a measure of the overall distance (approach) to the two asymptotes (the higher this value, the greater the distance to the asymptotes), $1/C_3$ is the slope (gradient) of the inclined asymptote and $x_0$ is the abscissa of the intersection of the two asymptotes. The values of these coefficients, pertaining to the particular NWP/WP/PM system, are: $x_0 = -4.3$, $C_0 = 0.003$, $C_3 = -1.16$. Note, eqn (13) is an implicit function of log*A* in terms of log*Ca*.

Using the analytical expressions from eqs (11) and (13) with the proper coefficient values, we may plot the fitted values of the reduced pressure gradient in terms of *Ca* and *r*, $x\left(Ca, r\right)$.

In the diagrams of Figure 3 we observe that not only the DeProF predicted values $x_{ij}(Ca_i, r_j)$ are recovered with great specificity, but the trend at extreme flow conditions, maintains its physically-true characteristics.

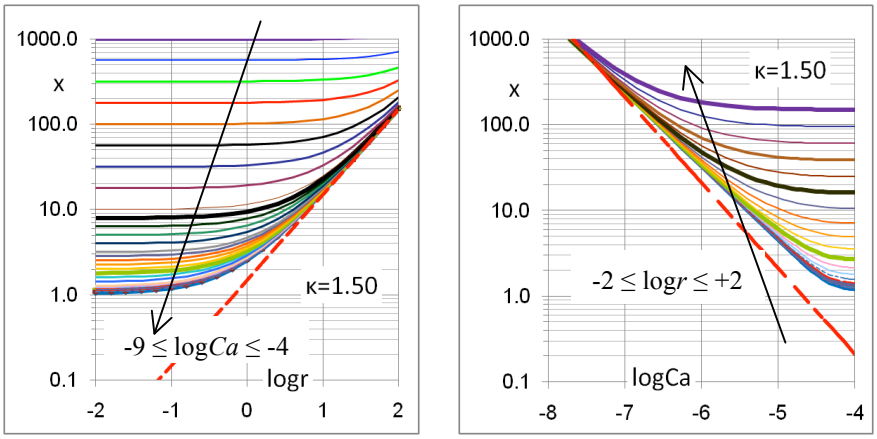


(a) (b)

**Figure 3** Plot of the reduced pressure gradient values, $x$, in terms of the flow set-up conditions, capillary number, $Ca$, and flow rate ratio, $r$. based on eqs (11) and (13), Table 1. (a) iso-$Ca$ curves; (b) iso-$r$ curves. Note, the iso-$Ca$ curves in (a) do not correspond to the iso-$Ca$ curves presented in **Figure 1**(b).

Plots of the relative permeability of the WP and the NWP, $k_{rw}$ and $k_{rn}$, in terms of log$Ca$ and log$r$, presented in Figure 4, can readily be produced using eqs (7) and (8).

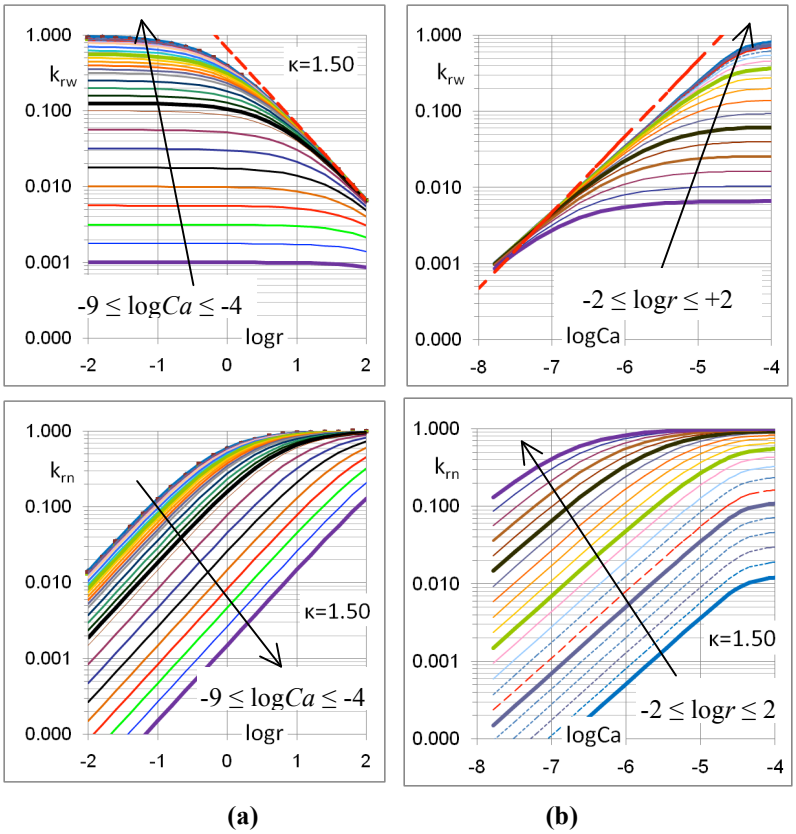


(a) (b)

**Figure 4**
Plots of the WP relative permeability, $k_{rw}$ (top row), and the NWP relative permeability, $k_{rn}$, (bottom row), in terms of the flow set-up conditions, capillary number, $Ca$, and flow rate ratio, $r$. Again, the two diagrams show: (a) iso-capillary curves; (b) iso-flow-rate-ratio-curves. Note, the $k_{rn}$ plots are scaled from the $k_{rw}$ plots according to the provision of eqn (8).

## CONCLUSION

Two-phase flow in porous media is burdened, not only with the bulk phase viscosities of NWP & WP, but also with the disconnection of the NWP and the associated capillarity effects induced by the formation of numerous NWP/WP menisci, that restrain and inhibit, to a certain extent, the superficial transport of NWP and WP. The momentum balance in the entire flow is regulated by the relative intensities of the NWP and WP flows (inducing Stokes flow viscous resistances within the bulk phases) and the degree of disconnection of the NWP (inducing Young-Laplace capillary resistance across the NWP/WP interfaces).

Results show the rheology of the NWP/WP/PM system shows a progressive mutation. In the ultra-low *Ca* regime the system shows a Bingham-fluid type rheology, whereby most of the disconnected NWP remains stranded. As *Ca* is progressively increased the flow attains a mixed capillarity to capillarity/viscosity dominated rheology. This is a result of the restructuring (reorganization) of the disconnected NWP flow into larger ganglia of increased mobility. With further increase in *Ca* the system attains – asymptotically- a Darcy-type flow rheology whereby the reduced pressure gradient becomes a linear function of flow rate intensities. The macroscopic phenomenology of the process described by the maps in Figures 1, 2 & 4 can be explained on the basis of the associated restructuring/reorganization of the NWP flow through connected and disconnected fractional flows [15].

The results suggest that it is possible to derive/use universal, true-to-mechanism functions of flow dependent relative permeabilities. Flow conditions are described by the flow intensities of the NWP and WP or, equivalently by the capillary number of the WP, *Ca*, and the NWP/WP flow rate ratio, *r*.

The proposed scaling function opens new possibilities in improving SCAL measurements by restructuring SCAL protocols in a smart way [11]. In addition, true-to-mechanism, flow dependent relative permeability maps may be incorporated in field-scale simulators and substantially improve their predictive capabilities/performance in terms of specificity.

## ACKNOWLEDGMENTS

The present work was partly supported by the Research Council of Norway through its Centres of Excellence funding scheme, project number 262644.

## REFERENCES

1. Avraam, D.G., Payatakes, A.C., 1995. Flow Regimes and Relative Permeabilities during Steady-State Two-Phase Flow in Porous Media. *J. Fluid Mech.* **293**, 207-236, doi: 10.1017/S0022112095001698
2. Avraam, D.G., Payatakes, A.C., 1999. Flow Mechanisms, Relative Permeabilities and Coupling Effects in Steady-State Two-Phase Flow in Porous Media. Case of Strong Wettability. *Industrial & Engineering Chemistry Research* **38**(3), 778-786. doi: 10.1021/ie980404o

3. Tsakiroglou, C.D., Avraam, D.G., Payatakes, A.C., 2007. Transient and steady-state relative permeabilities from two-phase flow experiments in planar pore networks. *Advances in Water Resources* **30**, 1981–1992. doi: 10.1016/j.advwatres.2007.04.002
4. Tallakstad, K.T., Knudsen, H.A., Ramstad, T., Løvoll, G., Maløy, K.J., Toussaint, R., Flekkøy, E.G., 2009. Steady-State Two-Phase Flow in Porous Media: Statistics and Transport Properties. *Physical Review Letters* **102** 074502, 1-4
5. Guillen V.R., Carvalho, M.S., Alvarado, V., 2012. Pore Scale and Macroscopic Displacement Mechanisms in Emulsion Flooding. *Transp. Porous Med.* **94**, 197–206 doi: 10.1007/s11242-012-9997-9
6. Georgiadis, A., Berg, S., Makurat, A., Maitland, G., Ott, H., 2013. Pore-scale microcomputed-tomography imaging: Nonwetting-phase cluster-size distribution during drainage and imbibitions. *Phys. Rev. E* **88**, 033002, 1-9, doi: 10.1103/PhysRevE.88.033002.
7. Aursjo, O., Erpelding, M., Tallakstad, K.T., Flekkøy, E.G., Hansen, A., Maloy, K.J., 2014. Film flow dominated simultaneous flow of two viscous incompressible fluids through a porous medium. *Frontiers in Physics* **2** (63), 1-9, doi: 10.3389/fphy.2014.00063
8. Datta, S.S., Ramakrishnan, T.S., Weitz, D.A., 2014. Mobilization of a trapped non-wetting fluid from a three dimensional porous medium, *Phys. Fluids* **26,** doi: 10.1063/1.4866641
9. Oughanem, R., Youssef, S., Bauer, D., Peysson, Y., Maire, E., Vizika, O., 2015. A Multi-Scale Investigation of Pore Structure Impact on the Mobilization of Trapped Oil by Surfactant Injection. *Transp. Porous Media* **109**, 673-692, doi: 10.1007/s11242-015-0542-5
10. Armstrong, R.T., McClure, J.E., Berrill, M.A., Rücker, M., Schlüter, S., Berg, S. (2016) Beyond Darcy's law: The role of phase topology and ganglion dynamics for two-fluid flow, *Phys. Rev. E* **94**, 043113, doi: 10.1103/PhysRevE.94.043113
11. Valavanides, M.S. 2018. Review of steady-state two-phase flow in porous media: independent variables, universal energy efficiency map, critical flow conditions, effective characterization of flow and pore network *Transp. in Porous Media* **123** (1), 42-99, doi: 10.1007/S11242-018-1026-1
12. Sinha, S., Hansen, A., 2012. Effective rheology of immiscible two-phase flow in porous media, *Europhysics Letters* **99** (4), 1-6, doi: 10.1209/0295-5075/99/44004
13. Sinha, S. Bender, A.T., Danczyk, M., Keepseagle, K., Prather, C.A., Bray, J.M., Thrane, L.W., Seymour, J.D., Codd, S.I., Hansen, A., 2017. Effective Rheology of Two-Phase Flow in Three-Dimensional Porous Media: Experiment and Simulation. *Transp. in Porous Media*, on line 6/2017, 1-18, doi: 10.1007/s11242-017-0874-4
14. Tsakiroglou, C.D., Aggelopoulos, C.A., Terzi, K., Avraam, D.G., Valavanides, M.S., 2015. Steady-state two-phase relative permeability functions of porous media: A revisit. *Int. J. Multiph. Flow* **73**, 34–42, doi: 10.1016/j.ijmultiphaseflow.2015.03.001
15. Valavanides, M.S., 2018. Oil fragmentation, interfacial surface transport and flow structure maps for two-phase flow in model pore networks. Predictions based on extensive, DeProF model simulations. *Oil & Gas Science and Technology - Rev. IFP Energies nouvelles* **73** (6), pp. 1-36, https://doi.org/10.2516/ogst/2017033